Stability of pole solutions for planar propagating flames

M. Rahibe,[1,2] N. Aubry,[1,2] and G. I. Sivashinsky[2,3]
[1]*Sibley School of Mechanical and Aerospace Engineering, Cornell University, Ithaca, New York 14853*
[2]*The Benjamin Levich Institute and the Mechanical Engineering Department, The City College of the City University of New York, New York, New York 10031*
[3]*School of Mathematical Sciences, Tel Aviv University, Ramat Aviv, Tel Aviv 69978, Israel*
(Received 26 February 1996; revised manuscript received 24 May 1996)

It is well known that the partial differential equation (PDE) describing the dynamics of a hydrodynamically unstable planar flame front admits exact pole solutions. For such solutions, the original PDE can be reduced to a set of ordinary differential equations (ODE's). The situation, however, is paradoxical since the steady solutions obtained by numerically integrating the PDE differ, in general, from the exact solutions governed by the ODE's. For example, if the initial condition is a one-pole steady solution, provided that the size of the domain considered is larger than a (small) critical length, the number of poles increases with time in the PDE while it remains constant in the ODE's. In previous studies, this generation of poles was thus believed to be an artifact or product of external noise, rather than a dynamical process intrinsic to the PDE. In this paper, we show that the phenomenon is due to the fact that most exact steady pole solutions are unstable for the PDE. In certain cases, such solutions are unstable for the ODE's, in other cases, they are neutrally stable for the ODE's but unstable for the PDE. The only steady pole solutions which are neutrally stable for both the ODE's and the PDE correspond to small interval lengths; both their number of poles and propagation speed are maximal (among all possible steady solutions corresponding to the interval considered) and all their poles are aligned on the same vertical axis in the complex plane (i.e., such solutions are coalescent). For a given interval of small length, there is only one such solution (up to translation symmetry). [S1063-651X(96)11710-4]

PACS number(s): 47.20.Ma, 82.40.Py, 47.20.Ky, 47.54.+r

I. INTRODUCTION

The dynamics of a planar wrinkled flame front subject to the Darrieus-Landau instability [1,2], under a weakly nonlinear approximation, is described by the evolution equation [3] which, in nondimensional variables, takes the form

$$\frac{\partial F}{\partial t}+\frac{1}{2}\left(\frac{\partial F}{\partial x}\right)^2=\frac{\partial^2 F}{\partial x^2}+\frac{\gamma}{2}I\{F\}. \tag{1}$$

Here, F is the dimensionless interface of the perturbed planar flame, in units of the width of the thermal flame structure l_T, t refers to the dimensionless time, in units of l_T/U_b, where U_b is the normal velocity of the flame front, and x is the spatial dimensionless coordinate, in units of l_T, defined over an interval of length L $(0\leqslant x\leqslant L)$. In this paper, L is considered finite and the flame front is assumed to be periodic, i.e.,

$$F(0)=F(L),\quad F_x(0)=F_x(L), \tag{2}$$

where F_x denotes the spatial derivative of F, i.e., $\partial F/\partial x$.

The parameter γ refers to the thermal expansion coefficient of the gas. The operator $I\{\ \}$ is a linear singular nonlocal operator which is responsible for the Darrieus-Landau instability [1,2]. It can be written as

$$I\{F\}=\frac{2}{L}\sum_{m=1}^{\infty}\widetilde{m}\int_0^L\cos[\widetilde{m}(x-\widetilde{x})]F(\widetilde{x},t)d\widetilde{x} \tag{3}$$

in physical space, or as

$$I\{\exp(i\widetilde{m}x)\}=|\widetilde{m}|\exp(i\widetilde{m}x) \tag{4}$$

in Fourier space. Here, $\widetilde{m}$ is the spatial wave number, defined as $\widetilde{m}=2\pi m/L$, where m is an integer.

We now mention two interesting properties of the partial differential equation (PDE) (1).

Property 1. The PDE (1) can be rewritten by using one parameter only (see also [4]). This can be achieved by rescaling the length L of the interval considered, so that it always takes the fixed value 2π. We then define the function Q by setting $Q(x)=F(Lx/2\pi)$, $0\leqslant x\leqslant 2\pi$. Substitution of this change of variable in (1) leads to the following PDE satisfied by Q:

$$\frac{\partial Q}{\partial t}+\frac{1}{2}\left(\frac{\partial Q}{\partial x}\right)^2=\frac{\partial^2 Q}{\partial x^2}+\frac{\widetilde{\gamma}}{2}I\{Q\}, \tag{5}$$

where $\widetilde{\gamma}=L\gamma/2\pi$. The boundary conditions become

$$Q(0)=Q(2\pi),\quad Q_x(0)=Q_x(2\pi). \tag{6}$$

However, in order to keep the notations used in previous publications [3,5], hereafter we return to the form (1) subject to the boundary conditions (2).

Property 2. There exists a symmetry among the set of solutions of the PDE (1) as the parameter L varies (for a fixed γ value). If $F_1(x,t)$ is a solution of (1) in the interval $[0,L_1]$, then $F_n(x,t)$ is a solution of (1) in the interval $[0,L_n]$ given by $F_n(x,t)=F_1(nx,t)$, where $L_n=nL_1$ and n is a positive integer.

Previous numerical integrations of the PDE (1) [5–7], hereafter referred to as ''direct numerical simulations

(DNS),'' have shown that cusps develop on the flame interface as time increases, even when the initial condition is chosen to be smooth. When the size of the spatial domain is relatively small, such a formation of new wrinkles occurs but is interrupted at a finite time: cusps eventually coalesce into one large peak. After this event, the shape of the front becomes frozen and the interface moves at a constant speed. In contrast, when the length L of the domain is relatively large, it seems that new cusps appear in a repetitive manner during the whole numerical integration [6,8] and that the flame speed increases. This wrinkling process, together with the speed enhancement, is similar to that observed in the study of outward propagating cylindrical flame [9,10]. There are, however, marked differences between the flame dynamics in the two geometries. In particular, for the cylindrical case there is no saturation of the flame speed. The latter undergoes a power-law acceleration in time.

The PDE governing the cylindrical flame [10] and that corresponding to a planar geometry (1) share another similarity: both equations have exact solutions which can be derived from a pole decomposition technique. For such pole solutions, the PDE formally reduces to a finite set of ordinary differential equations (ODE's) which describe the motion of the poles in the complex plane. Such poles are related to the cusps observed in physical space. By construction, the number of poles corresponding to the number of ODE's is fixed. However, numerical integrations of the original PDE show that, in most cases, even when the initial condition coincides with a pole solution, additional cusps keep forming on the interface. These new cusps are the signature of the appearance of additional poles in the complex plane. This phenomenon, apparently in contradiction with the pole decomposition method, has been considered to be an artifact generated by numerical noise alone [11,12]. It was then believed that a pseudorandom, noise-source term was needed in the PDE in order to correctly reproduce the generation of cusps [11]. Such new models were indeed found to lead to the rapid spawning of wrinkles.

It was shown in [10] that the stable solutions of the PDE describing the dynamics of a cylindrical wrinkled flame front are more complex than the exact pole solutions described earlier. This increase in the degree of complexity is due to the fact that (i) the exact pole solutions are unstable for the PDE, and (ii) when the initial condition is chosen to be a one-pole (exact) solution (presenting one cusp in physical space), the stable solution for the PDE consists of successive instabilities through which the flame front closely follows the one-pole exact solution before migrating to a three-pole exact solution. In the latter, the two new poles represent a pair of cusps located at symmetric positions on both sides of the initial cusp. This symmetric formation of cusps repeats and the front jumps to a five-pole exact solution, etc. More generally, the front follows the $(2N+1)$-pole solution (and its dynamics) before approaching and subsequently following the $(2N+3)$-pole solution. Such migrations are responsible for the repetitive formation of new cusps.

In this paper, we will see that the instability of exact pole solutions generally persists in the planar geometry (1) but the formation of new poles no longer occurs symmetrically with respect to existing poles at least in relatively small intervals. The planar front may thus jump from a one-pole exact solution to a two-pole exact solution.

Before we address this issue, we concentrate on the stability question of individual pole solutions and, in case of instability, we show that the appearance of new poles is intrinsic to the dynamics of the PDE (1) itself. In certain situations, the instability of such solutions is proved analytically. In all cases, we first perform direct numerical simulations (DNS) by integrating (1) numerically. Second, we carry out the linear stability analysis (LSA) by considering a perturbed pole solution and linearizing (1). The obtained equation is then integrated numerically for long times (until convergence of the solution is obtained). *All* our results (theoretical, numerical by DNS, and numerical by LSA) converge toward the same conclusions. For instance, we will show that all one-pole solutions are unstable, except one (for a given value of L) which is stable for $L<L_{c1}$ and becomes unstable for $L>L_{c1}$. The latter conclusion holds for two- and three-pole solutions if L_{c1} is replaced by L_{c2} and L_{c3}, respectively. The exact values of L_{cn} will be given below. We conjecture that this phenomenon can explain the systematic repetitive appearance of new poles for the cylindrical front [10] since the mean radius R of the latter plays the role of the length L which, in this case, keeps increasing with time $(R(t))$.

This paper is organized as follows. In Sec. II, we recall the expression of the pole solutions of the PDE (1) and present some analytical results regarding various steady states, including those originating in a coalescence process. We then consider the one- and two-pole solutions in Sec. III and address the stability issue of their steady states theoretically with respect to the set of ODE's. We then present solutions obtained by both direct numerical simulations of the PDE (1) and integrations of the ODE's. The linear stability problem of such pole solutions with respect to the PDE is addressed numerically in Sec. V. We then summarize our findings and conclude in the last section.

II. POLE SOLUTIONS AND STEADY STATES

In this section, we discuss the pole solutions of the PDE (1) in general and the coalescent states in particular. For the latter, all the poles are located on a vertical axis in the complex plane, at all times. We then concentrate on particular states, referred to as *steady states* for which the dynamics of the poles are time independent. Steady states can be either coalescent or noncoalescent.

A. Various pole solutions in physical space

1. General pole solutions

Exact solutions of the PDE (1) can be obtained by using the pole decomposition technique (see Joulin [7], Lee and Chen [13], Thual *et al.* [14], Minaev [15], and Renardy [4]).

We now recall the derivation of pole solutions (for more details, see [7,10,14]). For this purpose, we suppose that the space-time real-valued function

$$F(x,t)=C_N(k_0)t-2\sum_{\alpha=1}^{2N}\ln\left[\sin\left(\frac{kx-Z_\alpha(t)}{2}\right)\right] \qquad (7)$$

is a solution of the PDE (1). Here, k is the wave number $k=(2\pi/L)k_0$, k_0 being an integer, $C_N(k_0)$ is a constant, and $Z_{\alpha(t)}$ $[Z_\alpha(t)=a_\alpha(t)+ib_\alpha(t)]$ are poles in the complex plane. Notice that poles appear in pairs of complex conjugates in (7) since F is a real valued function. In addition, we note that in (7), we somehow disconnect the physical space from the complex plane where the poles are moving since $a_\alpha(t)$ belongs to the interval $[0,2\pi]$ (rather than $[0,L]$).

The dynamics of the poles $Z_\alpha(t)$ is obtained by substituting (7) in the PDE (1). This leads to the set of ODE's,

$$\dot{Z}_\alpha(t)=-k^2\sum_{\alpha\neq\beta}\cot\left(\frac{Z_\alpha-Z_\beta}{2}\right)-i\,\frac{\gamma k}{2}\,\mathrm{sgn}[\mathrm{Im}(Z_\alpha)], \quad (8)$$

where Im denotes the imaginary part and the function sgn has the usual meaning [sgn(0)=0 and sgn$(x)=|x|/x$ if $x\neq 0$]. The constant $C_N(k_0)$ takes the form

$$C_n(k_0)=kN(2kN-\gamma), \quad (9)$$

which depends, for a fixed γ value, on both the wavelength k and the number N of poles present in the particular pole solution considered.

We now derive additional useful analytical results regarding such solutions. For this purpose, we notice that *any* flame front satisfying the PDE (1) propagates downward since its average speed propagation is negative. This can be easily shown as follows. We first define the (spatial) average flame front $F(t)=(1/L)\int_0^L F(x,t)dx$. The expression of the mean speed of the flame front as

$$\dot{\bar{F}}(t)=\frac{d\overline{F(t)}}{dt}=-\frac{1}{2L}\int_0^L\left(\frac{\partial F}{\partial x}\right)^2(t)dx \quad (10)$$

can be easily deduced by taking the spatial average (over the period L) of (1). One can then see that $\dot{\bar{F}}(t)$ is necessarily negative.

This property, valid for any solution of (1), holds in particular for a pole solution (7). The mean speed of the latter can be written as

$$\dot{\bar{F}}(t)=C_N(k_0)-2\sum_{\alpha=1}^{N}\dot{b}_\alpha(t)\leqslant 0, \quad (11)$$

where $\dot{b}_\alpha(t)$ is the time derivative of the imaginary part of the pole $Z_\alpha(t)$.

2. Coalescent pole solutions

Among the set of pole solutions of the form (7), we now introduce a subset of solutions which play a particular role. According to a qualitative argument given by Thual *et al.* [14] for an infinitely large interval, two poles (isolated from the other existing poles) are attracted toward a line parallel to the imaginary axis in the complex plane. After the (vertical) alignment has occurred, the solution is called a *coalescent solution*. If, in addition, all the poles of such a solution are time independent, we say that we have a *coalescent steady state*. Note, however, that the corresponding front in physical space is not steady but spreads linearly in time: it is a standing wave with a frozen shape. Coalescent steady states have been observed in various numerical integrations of (1) where the length L is relatively small (see also our numerical simulations below, reported in Sec. IV): after their formation, all the cusps collide at the same spatial location(s) in physical space (note that, *a priori*, there may be various cusps in the interval of length L if k_0 is different from 1); after this collision time, the dynamics of the poles remains frozen and the front moves at a constant speed given by Eq. (9).

As in [14], we now rewrite the set of ODE's (8) in the particular case of coalescent solutions. Without loss of generality, we consider that the vertical axis containing all the poles coincides with the imaginary axis, that is, all the real parts of the poles, a_α, are equal to zero. In this case, the dynamics of the poles is governed by the set of ODE's,

$$\dot{b}_j=k^2\left\{\coth b_j+\sum_{\beta\neq j}\left[\coth\left(\frac{b_j+b_\beta}{2}\right)+\coth\left(\frac{b_j-b_\beta}{2}\right)\right]\right\}-\frac{\gamma k}{2}, \quad (12)$$

with $j=1,\ldots,N$. Note that, in this case, it suffices to consider the ODE's corresponding to the positive imaginary parts only, i.e., $b_j(t)>0$ for all times t, the complex conjugates being $-b_j(t)$.

3. Steady states

We now recall that a *steady state* is a pole solution of the form (7) for which all the poles are time independent. From the expression of the average speed of the front (9), applied to the particular case of steady states, it follows that the constant C_N is negative and that the number of poles is bounded, that is, $N\leqslant N_{\max}$, where the upper bound is given by

$$N_{\max}=\mathrm{Int}\left(\frac{\gamma}{2k}\right), \quad (13)$$

Int(x) denoting the integer part of the real number x.

We now consider particular steady states, those which are coalescent. By exploiting the similarity between the PDE (1) and that studied in [14], we adapt Thual *et al.*'s proof to show that there exist steady states for the set of ODE's (12) if the number N of poles present in the solution satisfies

$$N\leqslant N_0=\mathrm{Int}\left(\frac{\gamma}{4k}+\frac{1}{2}\right) \quad (14)$$

if $\gamma/4k+\frac{1}{2}$ is not an integer, and

$$N\leqslant N_0=\mathrm{Int}\left(\frac{\gamma}{4k}-\frac{1}{2}\right) \quad (15)$$

otherwise.

In addition, these coalescent steady states are stable for the dynamical system (12). The proof is not reproduced here since it is similar to that given in Appendix B of Ref. [14]. However, the stability of these states for the full set of ODE's (8) is still an open question, as is the stability of other steady states of (8).

A comparison between (13) and (14) shows that if, for certain values of the parameter γ/k, the maximal number of

poles in coalescent steady states is equal to one, $N_0=1$, then the maximal number of poles in *any* steady state is also equal to one, i.e., $N_{\max}=N_0=1$. We emphasize that this situation is met only for a very small range of values taken by γ/k ($2\leqslant\gamma/k<3$). Instead, if $N_0\geqslant 2$, then $N_{\max}$ is larger than N_0. This can be easily deduced from the fact that there exists an integer n such that $n\leqslant\gamma/2k<n+1$, or, equivalently, $(n+1)/2\leqslant\gamma/4k+\frac{1}{2}<n/2+1$. This means that, for given γ/k values, there may be noncoalescent steady states whose number of poles exceeds the number of poles present in coalescent steady states (except in the case where N_0 is equal to one).

B. Pole solutions in Fourier space

As in [10], it is very useful to write the Fourier transforms of the previous solutions in order to identify the latter in the results obtained by DNS. The Fourier transform of one-pole coalescent solutions (21) [4,10] is given by the expressions

$$\overline{F(t)}=\hat{F}_0(t)=C_1(k_0)t-2b(t)+4\ln 2 \tag{16}$$

and

$$\hat{F}_m(t)=\begin{cases}-\dfrac{2e^{-nb(t)}}{n} & \text{if } m=nk\\ 0 & \text{otherwise.}\end{cases} \tag{17}$$

More generally, pole solutions (7) can be rewritten as

$$F(x,t)=C_N(k_0)t-2\sum_{\alpha=1}^{N}\ln\tfrac{1}{2}\{\cosh b_\alpha(t)-\cos[kx+a_\alpha(t)]\} \tag{18}$$

and their Fourier transforms take the form

$$\hat{F}_m(t)=\begin{cases}-\dfrac{2}{n}\displaystyle\sum_{j}^{N}e^{-nb(t)}e^{-ina_j(t)} & \text{if } m=nk\\ 0 & \text{otherwise.}\end{cases} \tag{19}$$

The Fourier transform of any coalescent pole solution is real if $a_j(t)=0$ or π, as one can easily deduce by considering that all the a_α's are equal to zero or π in (18) and (19). This is particularly the case for one-pole solutions treated in Sec. III, for which the pole is located on one of these two lines (in the complex plane). As in [10], Fourier transforms will be very useful in identifying specific pole solutions in the numerical results of Sec. IV. Since identification criteria will also be obtained from other arguments explicitly used in Sec. IV, Fourier transforms will not be included in the set of figures retained in this manuscript.

III. ONE- AND TWO-POLE SOLUTIONS: ANALYTICAL RESULTS ON THE STABILITY OF STEADY STATES

In this section, we treat the case of one- and two-pole solutions explicitly. We first derive the set of ODE's governing the dynamics of such solutions and find the steady states of the dynamical systems thus derived. We then investigate the stability of these steady states analytically for the corresponding set of ODE's. On the one hand, it is clear that, if the solution is unstable for the ODE's, it will be unstable for the PDE as well. On the other hand, if the solution is either stable or neutrally stable for the ODE's, the stability question still remains open for the PDE. The latter will be addressed numerically in Sec. IV.

A. One-pole solutions

We first concentrate on the simplest coalescent pole solutions consisting of one pole and its conjugate [$Z(t)=a(t)\pm ib(t)$]. In this case, the PDE (1) formally reduces to the pole dynamics given by the two ODE's,

$$\begin{aligned}\dot{a}&=0,\\ \dot{b}&=k^2\coth b-\frac{\gamma k}{2},\end{aligned} \tag{20}$$

in which we choose $a=0$ (without loss of generality) and explicitly write the coalescent one-pole solution as

$$F(x,t)=C_1(k_0)t-2\ln\tfrac{1}{2}[\cosh b(t)-\cos(kx)], \tag{21}$$

where $C_1(k_0)=k(2k-\gamma)$.

As it is well known, one can easily see that the dynamical system (20) for one-pole solutions has a steady state defined by

$$b^*=\operatorname{arg\,coth}\left(\frac{\gamma}{2k}\right) \tag{22}$$

if $\gamma/2k>1$, which is in agreement with the two conditions (13) and (14), or (13) and (15). In addition, it is a stable coalescent steady state relative to the second ODE of (20) [14]. However, one can notice that it is only neutrally stable for the full dynamical system (20) including both ODE's. Indeed, the linearization of (20) around the equilibrium (a_0,b^*) (a_0 being a constant) leads to the two ODE's,

$$\begin{aligned}\dot{\tilde{a}}&=0,\\ \dot{\tilde{b}}&=-\frac{k}{\sinh^2 b^*}\,\tilde{b},\end{aligned} \tag{23}$$

where $\tilde{a}(0)$ and $\tilde{b}(0)$ are initial small perturbations around a_0 and b^*, respectively. We can thus see that one eigenvalue is strictly negative while the other one is zero. We emphasize here the fact that the dynamics of $a(t)$ is frozen (it is a constant) is valid for both the nonlinear and linear sets of ODE's (20) and (23).

B. Two-pole solutions

Here, we consider two-pole solutions ($N=2$) of the PDE (1). For such solutions, we know that the dynamics formally reduces to the set of ODE's (8). In this paragraph, we prove that there exists one and only one stable steady state (up to translations) with respect to the ODE's, for a given length L. This solution can be identified with the coalescent steady state. For this purpose, we introduce the two poles $Z_1(t)=a_1(t)+ib_1(t)$ and $Z_2(t)=a_2(t)+ib_2(t)$, which we

consider in the upper part of the complex plane [i.e., $b_1(t)$, $b_2(t)>0$ for all t]. Using (8), the dynamics of the real part of $Z_1(t)$ and $Z_2(t)$ are given by the two ODE's,

$$\dot{a}_1=-\dot{a}_2=-k^2\,\cot\left(\frac{a_1-a_2}{2}\right)G(a_1,a_2,b_1,b_2), \quad (24)$$

or

$$\dot{a}_1=-\dot{a}_2=-k^2\,\tan\left(\frac{a_1-a_2}{2}\right)H(a_1,a_2,b_1,b_2), \quad (25)$$

where the functions G and H are defined by the expressions

$$G(a_1,a_2,b_1,b_2)=\frac{\coth^2\left(\frac{b_1-b_2}{2}\right)-1}{\coth^2\left(\frac{b_1-b_2}{2}\right)+\cot^2\left(\frac{a_1-a_2}{2}\right)}+\frac{\coth^2\left(\frac{b_1+b_2}{2}\right)-1}{\coth^2\left(\frac{b_1+b_2}{2}\right)+\cot^2\left(\frac{a_1-a_2}{2}\right)} \quad (26)$$

and

$$H(a_1,a_2,b_1,b_2)=\frac{\tanh^2\left(\frac{b_1-b_2}{2}\right)-1}{\tanh^2\left(\frac{b_1-b_2}{2}\right)+\tan^2\left(\frac{a_1-a_2}{2}\right)}+\frac{\tanh^2\left(\frac{b_1+b_2}{2}\right)-1}{\tanh^2\left(\frac{b_1+b_2}{2}\right)+\tan^2\left(\frac{a_1-a_2}{2}\right)}. \quad (27)$$

Note that the functions G and H always take positive values and that the sets of the two ODE's (24) and (25) are equivalent. We, however, keep both formulations for the simplicity of the discussions.

The dynamics of the imaginary parts $b_1(t)$ and $b_2(t)$ of the poles are given by the two ODE's,

$$\dot{b}_1=k^2\left[\coth b_1+\coth\left(\frac{b_1-b_2}{2}\right)\frac{\coth^2\left(\frac{b_1-b_2}{2}\right)-1}{\coth^2\left(\frac{b_1-b_2}{2}\right)+\cot^2\left(\frac{a_1-a_2}{2}\right)}+\coth\left(\frac{b_1+b_2}{2}\right)\frac{\coth^2\left(\frac{b_1+b_2}{2}\right)-1}{\coth^2\left(\frac{b_1+b_2}{2}\right)+\cot^2\left(\frac{a_1-a_2}{2}\right)}\right]-\frac{\gamma k}{2} \quad (28)$$

and

$$\dot{b}_2=k^2\left[\coth b_1+\coth\left(\frac{b_1-b_2}{2}\right)\frac{\coth^2\left(\frac{b_1-b_2}{2}\right)-1}{\coth^2\left(\frac{b_1-b_2}{2}\right)+\cot^2\left(\frac{a_1-a_2}{2}\right)}+\coth\left(\frac{b_1+b_2}{2}\right)\frac{\coth^2\left(\frac{b_1+b_2}{2}\right)-1}{\coth^2\left(\frac{b_1+b_2}{2}\right)+\cot^2\left(\frac{a_1-a_2}{2}\right)}\right]-\frac{\gamma k}{2}. \quad (29)$$

In order to find the fixed point of this set of four ODE's describing the dynamics of the two poles, we first determine the equilibrium states of the real parts ($\dot{a}_i=0$, $i=1,2$). From (24) or (25), it is easy to deduce that there are only two equilibrium states. We now show that one of these fixed points is coalescent, while the other one is noncoalescent.

1. Coalescent steady states

The first fixed point has its two poles located on the same line parallel to the imaginary axis, i.e., $a_1=a_2$. In other words, it is a coalescent steady state. It follows that the imaginary parts b_1 and b_2 obey the new ODE's given by

$$\dot{b}_1=k^2\left[\coth b_1+\coth\left(\frac{b_1-b_2}{2}\right)+\coth\left(\frac{b_1+b_2}{2}\right)\right]-\frac{\gamma k}{2}, \quad (30)$$

$$\dot{b}_2=k^2\left[\coth b_2-\coth\left(\frac{b_1-b_2}{2}\right)+\coth\left(\frac{b_1+b_2}{2}\right)\right]-\frac{\gamma k}{2}.$$

These ODE's can also be deduced directly from (12). Then, it follows from [14] (see our discussion regarding coalescent steady states in Sec. II) that there exists a fixed point for the subset (30) and therefore for the complete set of ODE's (24), (25), (28), and (29) if $N_0\geqslant 2$.

2. Noncoalescent steady states

The second equilibrium for the real parts $a_i(t)$ $(i=1,2)$ is given by $|a_1-a_2|=\pi$. In physical space, this corresponds to two cusps located at a distance $L/2$ apart. In fact, it is possible to generalize this result to an N-pole solution, that is, there is always a steady state consisting of poles all aligned on two vertical axes $a_j=a_1$ or $a_j=a_1+\pi$ for all a_j. Returning to the case where $N=2$, the dynamics of the imaginary parts are given by the subsystem of ODE's,

$$\begin{aligned}\dot{b}_1&=k^2\left[\coth b_1+\tanh\left(\frac{b_1-b_2}{2}\right)+\tanh\left(\frac{b_1+b_2}{2}\right)\right]-\frac{\gamma k}{2},\\ \dot{b}_2&=k^2\left[\coth b_2-\tanh\left(\frac{b_1-b_2}{2}\right)+\tanh\left(\frac{b_1+b_2}{2}\right)\right]-\frac{\gamma k}{2}.\end{aligned}\tag{31}$$

Although finding the fixed points of the last equations is, in general, a nontrivial task, a particular equilibrium can be explicitly written when the two poles are at the same distance from the real axis, i.e., $b_1=b_2$. In this case, the equilibrium state can be written as $b_1=b_2=b^*$, where

$$b^*=\arg\coth\left[\frac{\gamma}{4k}+\frac{1}{2}\left(\frac{\gamma^2}{4k^2}-4\right)^{1/2}\right].\tag{32}$$

This equilibrium exists only if $\gamma/2k>2$, or $N_{\max}>2$. (Note here the condition regarding $N_{\max}$, rather than N_0.)

As we show in the next paragraph, the lack of explicit expression for noncoalescent fixed points in the general case where $b_1=b_1^*$ and $b_2=b_2^*$ will not affect our computation of the stability of the fixed points. We now concentrate on the latter.

3. Stability of the steady states for the ODEs

First, we investigate the linear stability of (general) noncoalescent steady states for the ODE's (24), (25), (28), and (29). We recall that the steady states considered here are defined by $|a_1-a_2|=\pi$, $b_1=b_1^*$, and $b_2=b_2^*$, where b_1^* and b_2^* are fixed points of the ODE's (28) and (29). We now consider a perturbed initial condition around this steady state and choose a disturbance which affects the real parts only, i.e.,

$$\begin{aligned}\tilde{a}_1(0)&=a_1+\delta a_1,\\ \tilde{a}_2(0)&=a_2+\delta a_2,\end{aligned}\tag{33}$$

where $\tilde{b}_1(0)=b_1^*$ and $\tilde{b}_2(0)=b_2^*$. Furthermore, we assume $|\tilde{a}_1(0)-\tilde{a}_2(0)|\neq\pi$.

Without loss of generality, we take $\tilde{a}_1$ and $\tilde{a}_2$ such that $0\leqslant\tilde{a}_1<\tilde{a}_2$. There are two possibilities, either $|\tilde{a}_2(0)-\tilde{a}_1(0)|<\pi$ or $|\tilde{a}_2(0)-\tilde{a}_1(0)|>\pi$, which we treat separately.

(i) $|\tilde{a}_2(0)-\tilde{a}_1(0)|<\pi$. Substitution of (33) in (25) implies that $\dot{\tilde{a}}_1>0$ and $\dot{\tilde{a}}_2<0$. Therefore, the two poles are approaching each other in the horizontal direction with the same speed. Thus the asymptotic state is a coalescent state with $\tilde{a}_1(t\to\infty)=\tilde{a}_2(t\to\infty)=[\tilde{a}_1(0)+\tilde{a}_2(0)]/2$.

(ii) $|\tilde{a}_2(0)-\tilde{a}_1(0)|>\pi$. Substitution of (33) in (25) implies that $\dot{\tilde{a}}_1<0$ and $\dot{\tilde{a}}_2>0$. Therefore, the two poles are moving away from each other at the same (but opposite) speed. They thus meet at the midpoint, independently of their initial positions since we have periodic boundary conditions. We can thus apply the same argument as in (i) and conclude that the asymptotic state is a coalescent state such that $\tilde{a}_1(t\to\infty)=\tilde{a}_2(t\to\infty)=[\tilde{a}_1(0)+\tilde{a}_2(0)+2\pi]/2$ if no boundary is crossed during the merging process or $\tilde{a}_1(t\to\infty)=\tilde{a}_2(t\to\infty)=[2\pi-\tilde{a}_1(0)+\tilde{a}_2(0)]/2$ if $\tilde{a}_1$ or/and $\tilde{a}_2$ have crossed the boundary as they coalesce.

It follows from (i) and (ii) that the noncoalescent states are all unstable. Note that we have used the full nonlinear equations to derive this result. Linearization was not necessary. In addition, our arguments are not restricted to steady states only and can be applied to unsteady solutions as well.

We now consider the coalescent states defined by poles whose real parts are equal $[a_1(0)=a_2(0)]$ and the imaginary parts $b_1(0)$ and $b_2(0)$ are fixed points for the ODE's (30). Here again, we use the analysis (i) made in the study of noncoalescent steady states to show that coalescent steady states are neutrally stable. For this purpose, we choose an initial condition which is a perturbed coalescent state [described by (33)] to which we can add a disturbance on the imaginary parts $b_i(t)$ of the poles. From point (i) above, it is straightforward to deduce that the asymptotic state is a coalescent state given by $\tilde{a}_1(t\to\infty)=\tilde{a}_2(t\to\infty)=[\tilde{a}_1(0)+\tilde{a}_2(0)]/2$. For nonsymmetrical perturbations such that $(\delta a_1\neq-\delta a_2)$, the new coalescent state is different from the initial condition: its location is at distance $[\delta a_1(0)+\delta a_2(0)]/2$ from the initial condition. The coalescent steady states are thus neutrally stable.

At this stage we can draw another important conclusion: for the two-pole system considered here, there is no stable periodic orbit since the two poles always tend to collide.

In conclusion, coalescent N-pole steady states are *neutrally* stable for the set of ODE's if $N_0\geqslant N$. For the one-(two-) pole solution discussed in this section, this condition becomes $N_0\geqslant 1$ $(N_0\geqslant 2)$. Stability (or neutral stability) for the set of ODE's, however, does not imply stability (or neutral stability) for the original PDE (1). We will show indeed in the next section that such steady states are, in general, unstable for the PDE. As far as the noncoalescent two-pole steady states are concerned, they are unstable for the set of ODE's, and therefore for the PDE (1) as well. All our numerical integrations, including those following the time history of perturbations presented in Sec. V, show that this result can be generalized to N-pole solutions, i.e., noncoalescent N-pole steady states are unstable.

IV. INVARIANT SUBSPACES FOR THE PDE AND NUMERICAL INTEGRATIONS

A. Invariant subspaces

As in [10], we identify two invariant subspaces for the PDE (1) which are used in our numerical integrations. In other words, if the initial condition $F(x,0)$ belongs to such a subspace, the solution $F(x,t)$ remains in that subspace *at all times*. These two subspaces are as follows.

(a) Σ_1, the set of functions F whose Fourier transform is real. If we consider the functions defined in the interval $[-L,+L]$, then Σ_1 coincides with the set of even functions.

(b) Σ_2, the set of functions F whose the only (possible) nonzero Fourier coefficients correspond to the wave numbers

nk (where n takes integer values).

The proof that these subspaces are invariant is the same as in [10]. The consideration of these two invariant subspaces, Σ_1 and Σ_2, is very useful in studying the role played by numerical noise in our problem. As it is well known, obtaining zero in numerical simulations is sometimes very difficult due to round-off errors. For instance the simple computation of the Fourier transform—computed by using the fast Fourier transform (FFT)—of the pole solution (21), shows the presence of spurious modes (see [10]). More precisely, the imaginary part of the Fourier coefficients is not equal to zero and the Fourier coefficients corresponding to wave numbers k' which are not multiples of k_0 (for $k_0 \geqslant 2$) are also nonzero.

In most numerical simulations reported in this paper, we use a one-pole solution (21) as the initial condition. The latter lies in both invariant subspaces, namely $\Sigma = \Sigma_1 \cap \Sigma_2$. At any later time, the solution of (1), therefore, should remain in Σ, if, of course, the latter is stable. If it is unstable, the slightest perturbation (in physical experiments) or round-off error (in numerical simulations) will carry the orbit away from the invariant subspace, toward a stable solution lying outside of this subspace. This remark allows us to follow the dynamics of the round-off errors outside $\Sigma_1 \oplus \Sigma_2$ during the numerical integration of (1). In some simulations, these errors remain below the level of the precision of the numerical scheme; this is the case when Σ is stable for (1). In other simulations, such errors grow, giving birth to new cusps and a new stable (steady or unsteady) state is reached at later times. When the latter situation is met, we also perform simulations by forcing the solution to remain in Σ at all times. In practice, we set all Fourier coefficients smaller, in absolute value, than a given threshold and of the imaginary part of all Fourier coefficients to zero. Of course, the threshold is machine and numerical scheme dependent; here, we take it as low as -28 in logarithmic (ln) scale since we use double precision.

B. Numerical scheme

The numerical scheme is the same as in [10], which is slightly different from the techniques used in [9,16]. It is based on a pseudospectral algorithm supplemented by the slaved-frog method for the advancement in time [16]. The iterative process used to integrate (1) is given by the equation

$$\hat{F}_m(t+\delta t) = \hat{F}_m(t-\delta t)\exp(2\omega_m \delta t) + \frac{\hat{G}_m(t)}{\omega_m}\left[1-\exp(2\omega_m \delta t)\right], \tag{34}$$

where

$$\omega_m = m\left(\frac{\gamma}{2} - m\right) \tag{35}$$

is the linear dispersion relation.

Here $\hat{F}_m(t)$ and $\hat{G}_m(t)$ denote the mth Fourier coefficients of the flame front $F(x,t)$ and the function $G(x,t)$, respectively. The latter is defined as $G(x,t) = -\frac{1}{2}(F_x(x,t))^2$. In the next paragraph, we present the results of our numerical integrations.

C. Results from numerical simulations

For the DNS reported here, the value of the thermal expansion coefficient γ is fixed to $\gamma = 1$. The total number of Fourier modes is maintained constant, $\mathcal{N} = 16\,384$, and the time step used is $\delta t = 0.01$. These two choices guarantee both the numerical convergence and a good precision of the flame front (particularly in Fourier space). The integration of the PDE (1) is performed over the time interval $0 \leqslant t \leqslant 2000$–$6000$. We also integrate the set of ODE's (8) or (20) subject to the same initial condition as in the integration of (1). For this, we use a Runge-Kutta-Merson method with the time step $\delta t = 0.1$ [17].

We first present a DNS for a small interval length $L = 4\pi$ whose stable solution is an unsteady state. This permits us to validate our DNS code since the latter solution is extremely close to that obtained by integrating the corresponding set of ODE's. We then present a few numerical simulations which illustrate the results of the previous sections by involving either stable or unstable steady states. We consider two interval lengths, $L = 14\pi$ and $L = 23\pi$. Initial conditions consist of either one-, two-, or three-pole solutions. We now present the results of a few simulations. Other simulations have been carried out, but since they confirm our conclusions, they are not reported here.

1. Simulation 1

In the first simulation, the wave number is $k_0 = 1$ and the length of the interval considered is $L = 4\pi$. In this case, the number of poles (13) and (14) are both equal to zero, i.e., $N_{\max} = N_0 = 0$. This implies that steady pole-solution states are not possible and, therefore, we expect the dynamics to be unsteady. The initial position of the pole is $b = 1.0$. Although we do not control any kind of noise in this computation, we find an excellent agreement between the pole dynamics, $b(t)$, obtained by DNS and that obtained from the ODE's (20) [see Fig. 1(a)]. Figure 1(b) shows that the computational noise outside of Σ_1 does not play any role since the imaginary part of all the Fourier coefficients of the numerically obtained solution have remained at the level of the background noise at $t = 4000$: Finally, Fig. 1(c) displays the flame front at time $t = 2000$. This first numerical experiment demonstrates the accuracy of our direct numerical simulation code, as well as the existence of unsteady solutions.

2. Simulation 2

In the second simulation, the initial condition is a (neutrally) stable coalescent steady state for the ODE's (20) for which the number of poles is maximal and the period coincides with the interval size L. The wave number is therefore $k_0 = 1$ and the length of the interval considered is $L = 6\pi$. It follows that the numbers of poles present in steady (noncoalescent and coalescent) solutions, $N_{\max}$ and N_0, are equal to one, i.e., $N_{\max} = N_0 = 1$. The position of the pole at $t = 0$ is chosen to be the value $b(0) = b^*$ given by (22), which is a fixed point for the ODE's (20). Once again, we carry out the DNS without controlling any kind of noise. As in Simulation 1, the integration of the PDE (1) and the integration of the set of ODE's (20) are in good agreement during the entire time of integration ($t = 0$–4000). Figure 2(a) shows that the speed of the mean flame front obtained from DNS coincides with

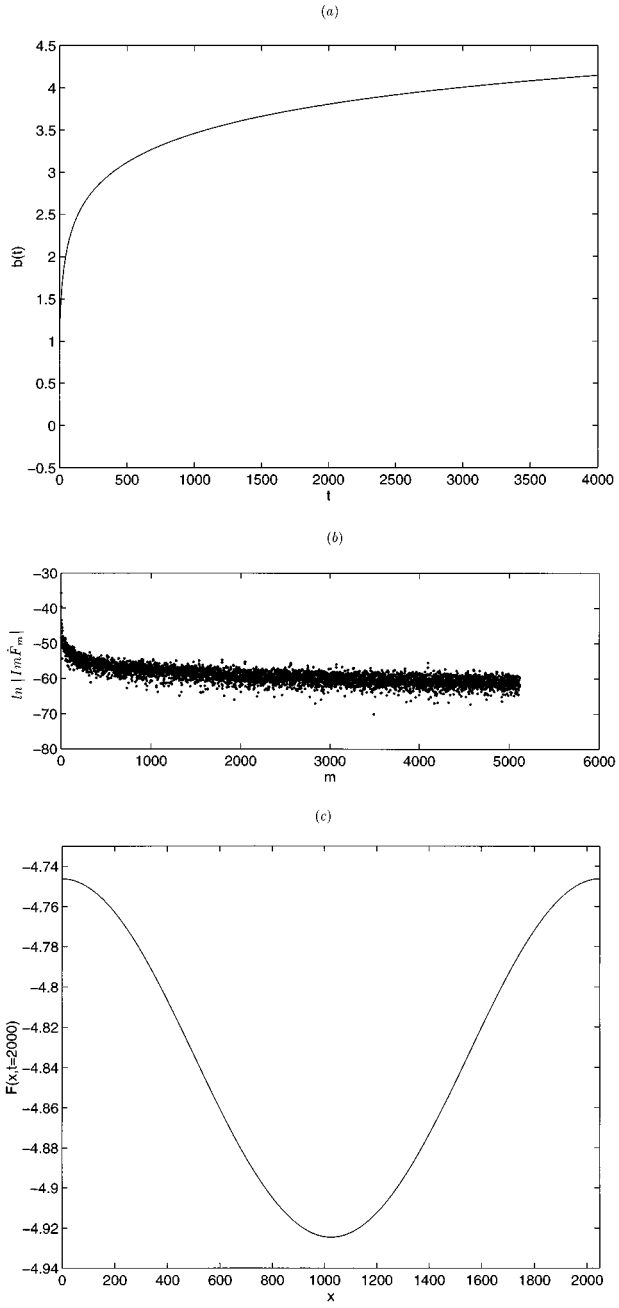

FIG. 1. Note: In all the figures representing the flame front in physical space, the label of the x axis indicates the number of points used in the simulations, rather than the actual length scale. In each case, the size of the interval considered is furnished in each figure caption. Simulation 1. Flame front dynamics in a domain of length $L=4\pi$. The initial condition is the one-pole solution of Sec. III with wave number $k_0=1$ and initial position of the pole $b_0(0)=1.0$. The solution obtained is a stable unsteady state: (a) The dynamics of the imaginary part of the pole $b(t)$ obtained by integration of the PDE (1) (solid line) without noise control and from the ODE's (dashed line). Both curves coincide; (b) the imaginary part of the Fourier coefficients at time $t=4000$ showing that the invariant subspace Σ_1 is stable; (c) flame front at time $t=2000$.

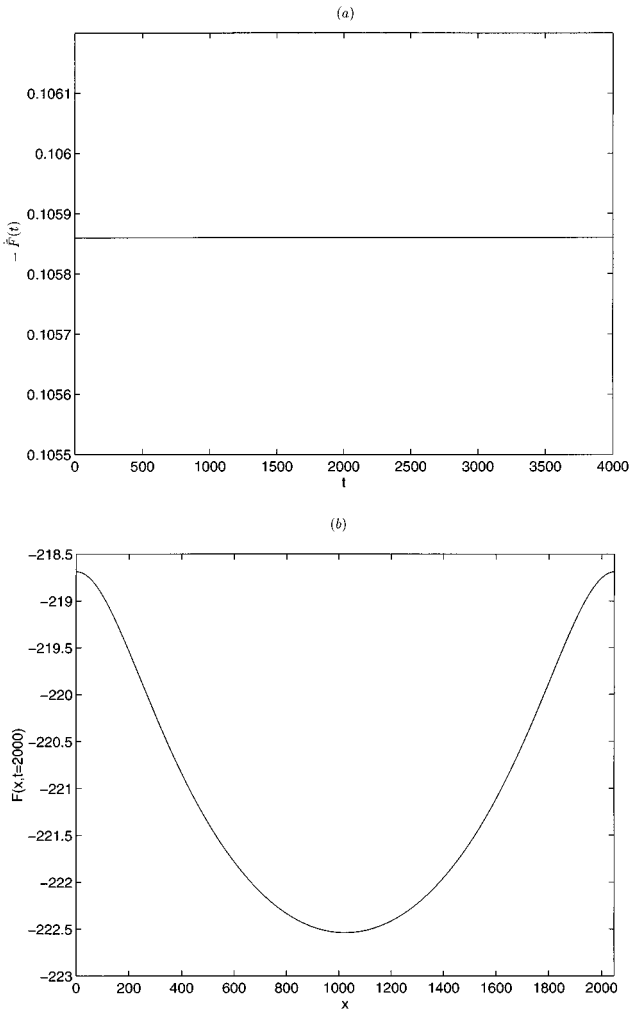

FIG. 2. Simulation 2. Flame front dynamics in a domain of length $L=6\pi$. The initial condition is the one-pole solution of Sec. III with wave number $k_0=1$ and initial position of the pole $b_0(0)=b^*$. This initial condition is stable for both the ODE's and the PDE (see Sec. V). (a) The speed (in absolute value) of the mean flame front, $-\dot{\bar{F}}(t)$, obtained by integration of the PDE (1) (solid line) without noise control and from the ODE's (dashed line). Both curves coincide; (b) the flame front at time $t=2000$.

the analytical expression of the fixed point of the ODE's [i.e., $\dot{\bar{F}}(t)=dF/dt=C_1(k_0=1)$], the discrepancy being 6.1×10^{-15} after $t=200$. A graph of the imaginary part of the Fourier spectrum, not shown here since it is similar to that obtained for Simulation 1 [Fig. 1(b)], confirms that the solution remains in the invariant subspace Σ_1. Figure 2(b) displays the flame front at time $t=2000$. The shape of the front is frozen at later times, until the end of our simulation ($t=4000$). It is clear that, for the interval of length L and wave number k_0 considered here, the one-pole solution whose pole location is given by (22) is a stable solution for the PDE (1). The next simulations, however, show that this situation is very particular; it is due to the following conditions simultaneously met: (i) the number of poles N present in the steady state is N_0, (ii) all the poles are aligned on a vertical axis in the complex plane (the solution is coalescent), (iii) the period of the solution coincides with the length L of the interval, and (iv) the length L is relatively small.

It is clear that, for all interval sizes L such that N_0 keeps the same value, i.e., $4\pi<L\leqslant12\pi$, the present initial condition remains neutrally stable for the PDE. We confirmed this point by carrying out the DNS over an interval of length

$L=5.75\pi$, a value particularly useful for the discussion of Simulation 3 below: the ($N_0=1$, $k_0=1$)-pole solution is indeed neutrally stable in this simulation as well. We now demonstrate that stability for the PDE is a particular situation by reporting the following simulations.

3. Simulation 3

This simulation and the next ones are slight modifications of Simulation 2. Both show evidence of pole solutions that are (neutrally) stable for the ODE's but *unstable* for the PDE. Here again, the initial condition is a (neutrally) stable coalescent equilibrium for the ODE's (20) for which the number of poles is maximal. The period of this solution, however, is smaller than L. The only parameters different from those used in Simulation 2 are the wave number k_0 of the initial one-pole solution and the length L of the interval. The new values are $k_0=4$ (making the period equal to $L/4$) and $L=23\pi$. It follows that the maximal numbers of poles in (coalescent and noncoalescent) steady solutions are, once again, equal to one, i.e., $N_0=N_{\max}=1$. As before, the initial position of the pole is $b(0)=b^*$, where b^* is given by (22).

We first perform an integration of the PDE (1) by applying our noise filtering technique, which, we recall, consists in maintaining the solution inside the invariant subspace Σ at all times. Within this subspace, we expect such a solution to be stable for the PDE (1), which is indeed confirmed numerically. The comparison between these numerical results and the theoretical analysis of the ODE's (8) shows an excellent agreement. As in Fig. 2(a), the velocity of the averaged flame front obtained from the (filtered) integration of the PDE is observed to be a constant, very close to the analytical result obtained with the ODE's, $\dot{F}=dF/dt=C_1(k_0=4)$. More precisely, the difference between the theoretical result and the asymptotic value obtained after $t=200$ by filtered DNS is 1.1×10^{-16}. Figure 3(a) shows the frozen shape of the flame front at $t=2000$. We conclude that the one-pole solution of wave number $k_0=4$ is stable within the subspace Σ. Such a result was expected from the result of the previous simulation and Property (2) of Sec. I: the global symmetry among the set of solutions as L varies makes the one-pole solution of period $L=5.75\pi$ in an interval $[0,L]$ comparable to the one-pole solution of period $L=L'/4$ in the interval $[0,L']$, where $L'=23\pi$. The symmetry implies that the stability of the two solutions should also be the same within the subspaces $\Sigma_2(k_0=1)$ corresponding to L and $\Sigma_2(k_0=4)$ corresponding to $L'=4L$. While $\Sigma_2(k_0=1)$ contains functions with all wave numbers, $\Sigma_2(k_0=4)$ is restricted to functions whose wave numbers k_0 are multiples of 4 only. In other words, the symmetry does not allow us to deduce the stability of the second solution *in the full space* from the stability of the first solution. We now address this issue by reiterating our DNS without noise filtering technique, thus allowing perturbations to grow away from Σ.

Such a DNS shows that round-off errors outside of the subspace $\Sigma_1\oplus\Sigma_2$ grow, leading to the formation of new cusps. In this case, it is clear that the solution obtained from the PDE is substantially different from that obtained from the ODE's. Figures 3(b)–3(e) clearly show this instability by representing the flame front at various times ($t=600$, 800, 1000, and 1200). In Fig. 3(c), only two cusps are present. This solution is identified with a two-pole solution.

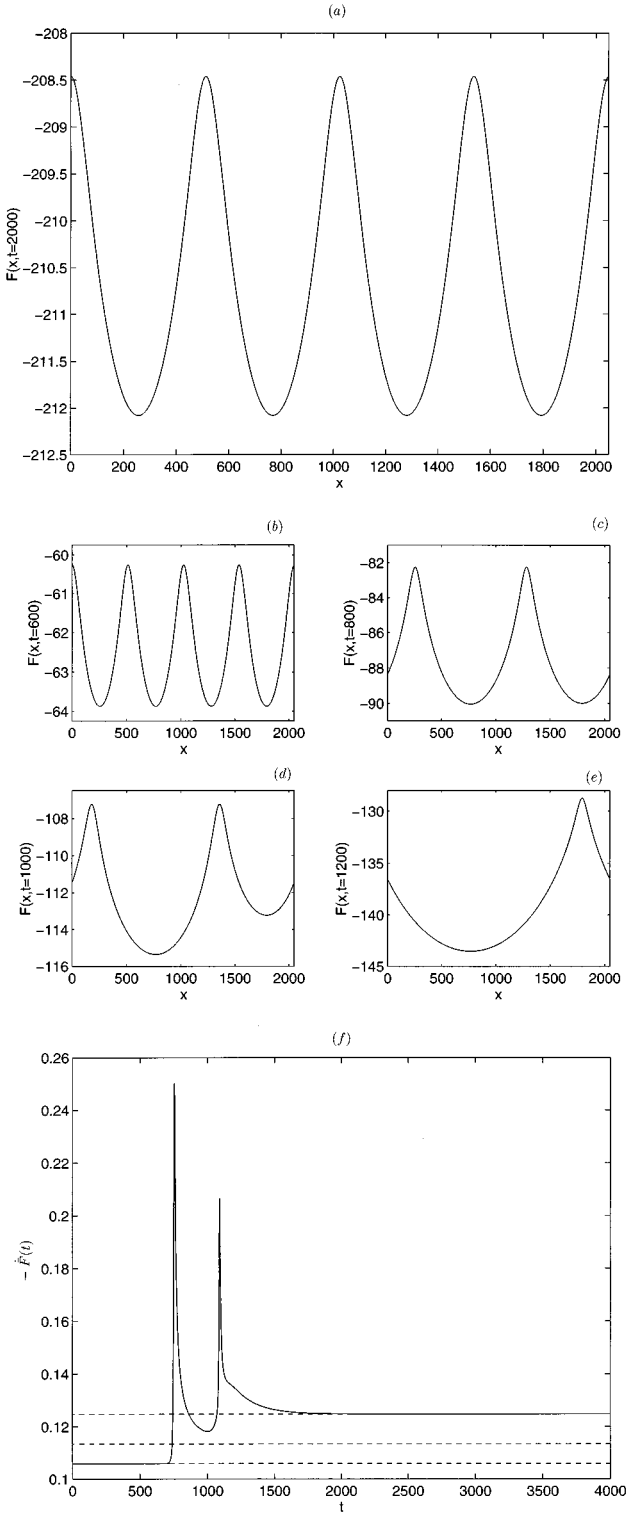

FIG. 3. Simulation 3. Flame front dynamics in a domain of length $L=23\pi$. The initial condition is the one-pole solution of Sec. III with wave number $k_0=4$ and initial position of the pole $b_0(0)=b^*$. (a) Numerical integration of the PDE (1) with noise control: the initial condition is stable. (a) The flame front at time $t=2000$; (b)–(f) Numerical integration of the PDE without noise control: (b)–(e) flame front at various times showing the (successive) presence of four peaks, two peaks, and finally one peak only, (f) the speed (in absolute value) of the mean flame front $-\dot{F}(t)$ (solid line) compared with the theoretical values $-C_1(k_0=1)$, $-C_2(k_0=1)$, and $-C_3(k_0=1)$ of the steady one-pole, two-pole, and three-pole solutions computed from the ODE's (dashed lines).

At birth, the two cusps are $L/2$ apart in physical space (and therefore $|a_1-a_2|=\pi$ for the real parts of the two corresponding poles). In Fig. 3(c), the distance between the two cusps is slightly larger than $L/2$ (by approximately 4%). At later times [see Fig. 3(d)], the two poles are going away from each other. This behavior is consistent with our analysis of the ODE's (8) governing the dynamics of two poles ($N=2$). At time $t=1200$, the two poles have collided [Fig. 3(e)]. The corresponding solution, however, has three poles rather than only two, as we now discuss. Figure 3(f) displays the speed of the mean front, $-\dot{\bar{F}}(t)$, computed numerically by DNS. In the same figure, horizontal dashed lines represent the constant velocity values $-C_1(k_0=4)$, $-C_2(k_0=1)$, and $-C_3(k_0=1)$ for comparison. As expected, the speed coincides with $C_1(k_0=4)$ for a relatively long time during which the computed solution stays close to the ($N=1$, $k_0=4$)-pole solution. The front then undergoes an important acceleration (in absolute value) which manifests itself as a sudden and abrupt increase (in absolute value) in the front speed. The front then slows down considerably and the speed decreases (in absolute value) to a value slightly larger than $-C_2(k_0=1)$. Such a burst in the front speed corresponds to the instability undergone by the solution: the solution jumps from the neighborhood of the one-pole solution to the neighborhood of the two-pole solution. The latter corresponds to the shape of a front displayed in Fig. 3(c). After $t=1000$, the front undergoes another instability and a second burst appears in the velocity of the mean front which finally reaches the value $-C_3(k_0=1)$ [Fig. 3(f)]. The computed solution has clearly migrated (through successive steps) from a two-pole solution to a three-pole solution. The latter is a coalescent steady state which is stable for both the ODE's (see Sec. III) and the PDE. At later times, the front moves at constant speed without deformation. In order to confirm our findings, we now give the precise numerical values found by fitting $\dot{\bar{F}}(t)$ obtained from DNS in the time intervals $T_1=[0,500]$ and $T_2=[3000,4000]$; we obtain $\dot{\bar{F}}_{T_1}=-0.105\,860\,113\,434\,87$ and $\dot{\bar{F}}_{T_2}=-0.124\,766\,373\,167\,788$, respectively. These values coincide with the theoretical values $C_1(4)$ and $C_3(1)$, up to 3×10^{-12} and 2×10^{-8}, respectively. The various plateaus visited by the front speed as time increases [see also Fig. 4(g) below] were observed in previous numerical simulations [7].

Note that, in the case of the present simulation, we had computed the maximal numbers of poles, N_0 and $N_{\max}$, permitted by the length of the interval considered. This computation was performed for solutions of wave number $k_0=4$. In this situation, we recall that $N_0=N_{\max}=1$. Note that, if we allow a wave number instability to occur (as we did in our second numerical integration by relaxing the noise filter), thereby permitting the wave number to become $k_0=1$ (corresponding to a transfer of energy toward large scales), then N_0 and $N_{\max}$ become $N_0=3$ and $N_{\max}=5$. The fact that the ($N=N_0=3$, $k_0=1$) coalescent steady pole solution is stable is consistent with the result obtained in Simulation 2. In both simulations, the coalescent N_0-pole steady solution of (smallest) period L is (neutrally) stable. For a given interval of length L, the solution always goes to a coalescent steady solution containing as many poles as possible, and progressing as fast as possible (the front speed is maximal among all possible steady solutions).

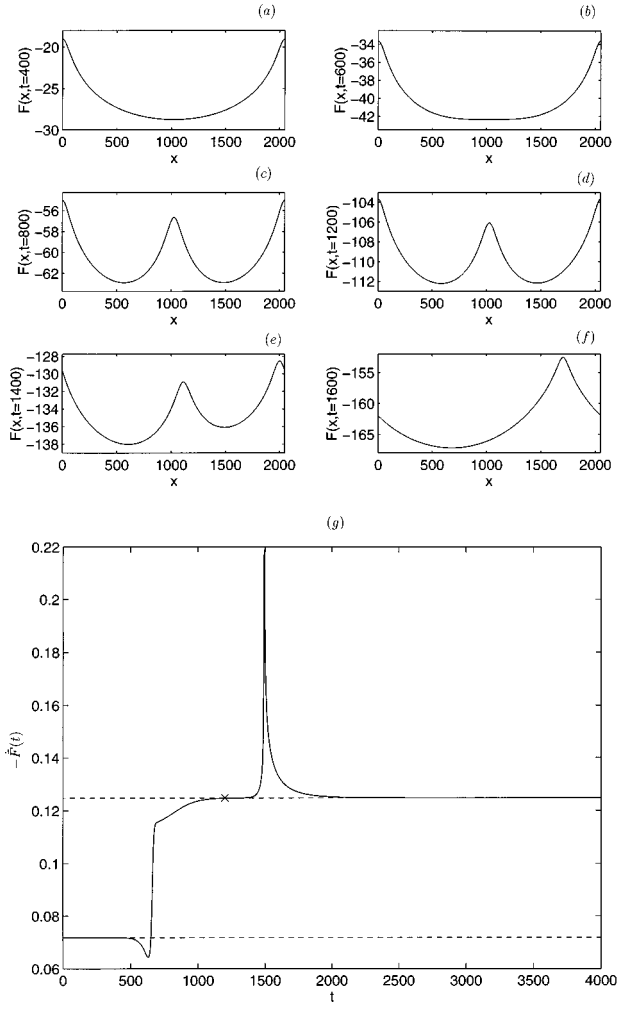

FIG. 4. Simulation 4. Flame front dynamics in a domain of length $L=23\pi$. The initial condition is the one-pole solution with wave number $k_0=1$ and initial position of the pole $b_0=b^*$. (a)–(f) The flame front at various times showing the presence of one peak, the formation of a second peak, and the coalescence of the two peaks. (g) The speed (in absolute value) of the mean flame front $-\dot{\bar{F}}(t)$ (solid line) compared with the theoretical values $-C_1(k_0=1)$ and $-C_3(k_0=1)$ of the steady one-pole and three-pole solutions computed from the ODE's (dashed lines). The cross indicates the instant $t=1200$ [corresponding to (d)].

4. Simulation 4

Our fourth simulation is identical to Simulation 3, except that the wave number of the initial one-pole solution is now $k_0=1$. We recall that the initial condition is stable for the set of ODE's and that the maximal numbers of poles is $N_0=3$ for coalescent steady states and $N_{\max}=5$ for noncoalescent steady states. In this computation, we do not apply any noise control technique. Once again, the results clearly show discrepancy between the integration of the PDE and that of the ODE's (20), supporting the fact that the initial condition, stable for the ODE's, is unstable for the PDE. Indeed, after a certain time, new poles appear, manifesting themselves as a new cusp in physical space. Figures 4(a)–4(f) show the evolution of the flame front as time increases. At time $t=400$ [Fig. 4(a)], the solution is still well described by the one-pole ($k_0=1$) equilibrium of the ODE's. At time $t=600$ [Fig. 4(b)],

the front flattens around the midpoint $x=L/2$ in the interval considered. The appearance of a new cusp at this location is clear at time $t=800$ [Fig. 4(c)]. This new cusp does not appear alone, but together with another one located at $x=0$. We suspect that the two cusps appear simultaneously, a conjecture supported by both our discussion of Fig. 4(g) below and the stability analysis performed in Sec. V. We recall that such a three-pole solution for which $a_1=a_2=0$ and $a_3=\pi$ is a possible (noncoalescent) equilibrium for the three-pole system of ODE's (see Sec. III). As discussed in Sec. III, the noncoalescent three-pole steady state is unstable and the collision process takes place in Fig. 4(d) and 4(e). Figure 4(f) shows the front at time $t=1600$. At that time, the solution has reached a stable coalescent three-pole steady solution, which is identical to the final state obtained in Simulation 3. Figure 4(g) permits us to compare the time derivative of the mean front $\dot{F}(t)$ obtained by DNS and the (theoretical) constant speed of the one-pole and three-pole steady solutions $C_1(k_0=1)$ and $C_3(k_0=1)$ (the cross in this figure highlights the value at time $t=1200$). As in Simulation 3, the various instabilities manifest themselves as jumps or bursts. This figure gives further evidence to the fact that the two new poles appear simultaneously and that the solution numerically obtained jumps from the neighborhood of a one-pole steady solution to the neighborhood of a three-pole steady solution; none of the steady two-pole solutions seems to be approached in this simulation. The solution stays very close to the steady $(N=1,\ k_0=1)$-pole solution for a relatively long time, as shown by the numerical value $\dot{F}=-0.124\,763\,705\,104\,522$ (obtained in the time interval [0,300]) which is equal to the theoretical speed of the one-pole steady state, $C_1(k_0=1)$, with an accuracy of 10^{-7}. The presence of three poles after the first instability is also confirmed by the precise measurement of the time derivative of the mean front obtained numerically. Indeed, we find $\dot{F}(t=1200)=-0.124\,763\,705\,104\,522$, which is equal to the theoretical speed of the three-pole steady state, $C_3(k_0=1)$, with an accuracy of 2×10^{-12}. After the second instability (in the time interval [3000,4000]), the numerical value becomes $\dot{F}=-0.124\,763\,821\,337\,76$ (measured in the time interval [3000,4000]), which, again, is very close to $C_3(k_0=1)$, up to a precision of 10^{-7}.

5. Simulation 5

In this simulation, the initial condition is the asymptotic state obtained in Simulations 3 and 4. We recall that this is a coalescent three-pole steady state $(N=3,\ k_0=1)$ for the interval of length $L=23\pi$. In this case, the steady state has the maximal period and the maximal number of poles N_0 allowed. This simulation confirms our previous findings that it is stable for the PDE. Graphs, not shown here since they are similar to Fig. 2(a) and 1(b), prove that the speed $\dot{F}(t)$ is constant (very close to the theoretical value obtained from the ODE's, the difference being 3.9×10^{-13} after $t=1500$) and that the numerical noise in the imaginary part of the Fourier coefficients remains very small at all times.

6. Conclusions on simulations

Additional tests have been carried out. First, simulations have been performed for an interval of length $L=14\pi$. Only the coalescent two-pole solution with wave number $k_0=1$ has been found to be neutrally stable; all other initial conditions corresponding to steady exact pole solutions are unstable. Second, for the three lengths reported in this section $(L=6\pi,\ L=14\pi,\ L=23\pi)$, all exact pole solutions stable for the corresponding ODE's have been chosen as initial conditions. They are all unstable, except the coalescent N_0-pole solutions for which the wave number is $k_0=1$, which is neutrally stable. Note that, among such solutions, for a given length L, there are two states which move at a maximal speed (in absolute value): the $(N=N_0,\ k_0=1)$-pole solution and the $(N=1,\ k_0=N_0)$-pole solution. The latter, however, is unstable for sufficiently large intervals $(L>12\pi$, i.e., as soon as $N_0>1)$. It is interesting to note that the system selects both the largest number of poles (for coalescent solutions) and the maximal speed.

V. LINEAR STABILITY ANALYSIS

As we have seen in our direct simulations of the PDE (1), a large number of steady states of the set of ODE's (20) seems to be unstable for the PDE (1). In this section, we address the linear stability of these solutions directly. For this purpose, we decompose the solution into the (known) steady state and a perturbation, substitute this decomposition into the original PDE (1), and retain the linear terms only [18,19]. We then integrate the linear PDE thus obtained numerically.

In all our numerical simulations, the perturbation exhibits an asymptotic state of the form $u(x,t)=e^{\lambda t}v(x)$, where λ is a real number. When λ is positive for large times t, the steady state is said to be *unstable*. The mode $v(x)$ corresponds to the linearly most unstable mode and λ is its growth rate. The steady state is said to be *stable* when λ is negative and *neutrally stable* when λ is zero. We emphasize that we do not impose *a priori* a particular form for $v(x)$. It is worth mentioning that this technique can be applied to the stability analysis of unsteady solutions, and is not restricted to steady states only. Notice that λ is the PDE counterpart of the (largest) Lyapunov exponent used in temporal dynamical systems theory [20–23]. Recently, the notion of Lyapunov exponents has indeed been used for PDE's, e.g., for the Kuramoto-Sivashinsky [24] and the Navier-Stokes equations [25]. As in the case of the numerical computation of Lyapunov exponents, λ must be independent of the initial perturbation [20,22]. This property is satisfied in our numerical experiments. In practice, we follow the temporal behavior of the energy of the perturbation, defined by

$$R(t)=\int_0^L [u^2(x,t)]dx, \tag{36}$$

whose (asymptotic) exponent β is twice that of $u(x,t)$, that is, for large times $R(t)$ is proportional to $e^{\beta t}$ with $\beta=2\lambda$. In our numerical simulations, we consider β rather than λ.

We consider a steady pole solution $u_0(x,t)$ and perturb the flame front around $u_0(x,t)$, so that $F(x,t)=u_0(x,t)+u(x,t)$, where $u(x,t)$ is a perturbation. By neglecting the nonlinear term $(u_x)^2$, we obtain the linear PDE [18,19],

$$\frac{\partial u}{\partial t}+\frac{\partial u_0}{\partial x}\frac{\partial u}{\partial x}=\frac{\partial^2 u}{\partial x^2}+\frac{\gamma}{2}I\{u\}, \tag{37}$$

where $I\{\}$ is the operator defined by (3). It is straightforward to see that constant functions are trivial solutions of (37).

We then seek other solutions numerically. For this, we apply the same numerical scheme as for the numerical integration of the original, nonlinear PDE (1). More precisely, the following iteration process is used:

$$\hat{u}_m(t+\delta t)=\hat{u}_m(t)\exp(2\omega_m\delta t)+\frac{\hat{P}_m(t)}{\omega_m}[1-\exp(2\omega_m\delta t)], \tag{38}$$

where ω_m is given by the dispersion relation (35) and $u_m(t)$ and $P_m(t)$ denote the Fourier coefficients of the perturbation $u(x,t)$ and $P(x,t)=-(\partial u_0/\partial x)(\partial u/\partial x)$, respectively.

In the present computations, we keep the total number $\mathcal{N}$ of Fourier coefficients identical to that used in the numerical integration of the original PDE. However, in most cases, we repeated our runs with a different number of Fourier coefficients in order to guarantee that numerical convergence is reached.

We now list some of the initial perturbations we use in our computations:

$$\begin{aligned} u_1(x,0)&=\sin kx+\cos kx+0.5(\sin 2kx+\cos 2kx),\\ u_2(x,0)&=\sin kx+0.5\,\sin 2kx,\\ u_3(x,0)&=\cosh(\sin kx),\\ u_4(x,0)&=1+0.5\,\cos kx, \end{aligned} \tag{39}$$

where we recall that $k=2\pi k_0/L$ and $k_0=1,2$, except for $u_2(x,t)$, in which $k_0=1$. All the previous perturbations have been used to check that the exponent β (or, equivalently, λ) is independent of the particular initial condition chosen. They also give an indication of the dimension of the eigenspace corresponding to λ. We will come back to this point in the discussion below.

Notice that the linearized PDE (37) has also a trivial solution, the constant function, which is associated with the exponent $\lambda_0=0$. This point is due to the invariance of the PDE (1) under shifts in the function F, i.e., if $F(x,t)$ is a solution of the PDE (1), then the function $F(x,t)+c$ (c being a constant) is also a solution of (1).

In our present computations, we solve the linearized PDE (37) for all the cases studied in Sec. IV by DNS. All the stability results of the present section agree with the conclusions drawn in Sec. IV. We now select a few typical cases relative to both unstable and stable steady states.

A. Unstable steady states

We first investigate the linear stability of the initial condition of Simulation 3 (see Sec. IV). We recall that this reference state is the one-pole solution ($N=1$, $k_0=4$), stable for the corresponding set of ODE's. Here, we use all four functions $u_1(x,t)$, $u_2(x,t)$, $u_3(x,t)$, and $u_4(x,t)$ as initial conditions and obtain identical results for the exponent λ and the corresponding mode $v(x)$. Figure 5 reports the spatiotemporal behavior of the perturbation $u(x,t)$. Figure 5(a) shows that the energy of the perturbation grows exponentially fast, after a short transient. Figure 5(b) displays the normalized perturbation $u(x,t)/\sqrt{R(t)}$ at various times in the time interval [3000,4000]. The superimposition of the various profiles demonstrates that such a quantity becomes time independent for large times and that the perturbation can be written as $u(x,t)=e^{\lambda t}v(x)$, in which the exponent λ is positive. The reference state is then linearly unstable. Like the reference state, the function $v(x)$ has four cusps and it is periodic, but its period is no longer $L/4$ (as in the reference solution) but $L/2$, indicating a subharmonic instability. Fourier mode multiples of $k_0=2$ gain energy. This is consistent with the fact that the reference state is stable in the subspace Σ, but unstable outside of Σ, as shown by our DNS with noise control. We find $\beta=2\lambda=0.084\,720\,3$ from Fig. 5(a). The simulations, first performed with $\mathcal{N}=16\,384$ Fourier modes, were repeated with $\mathcal{N}=8192$ modes. The two sets of computations lead to identical results; in particular, the $\ln R(t)$ curves obtained in the two cases are superimposed. The linearly most unstable mode $v(x)$ resulting from both computations is also

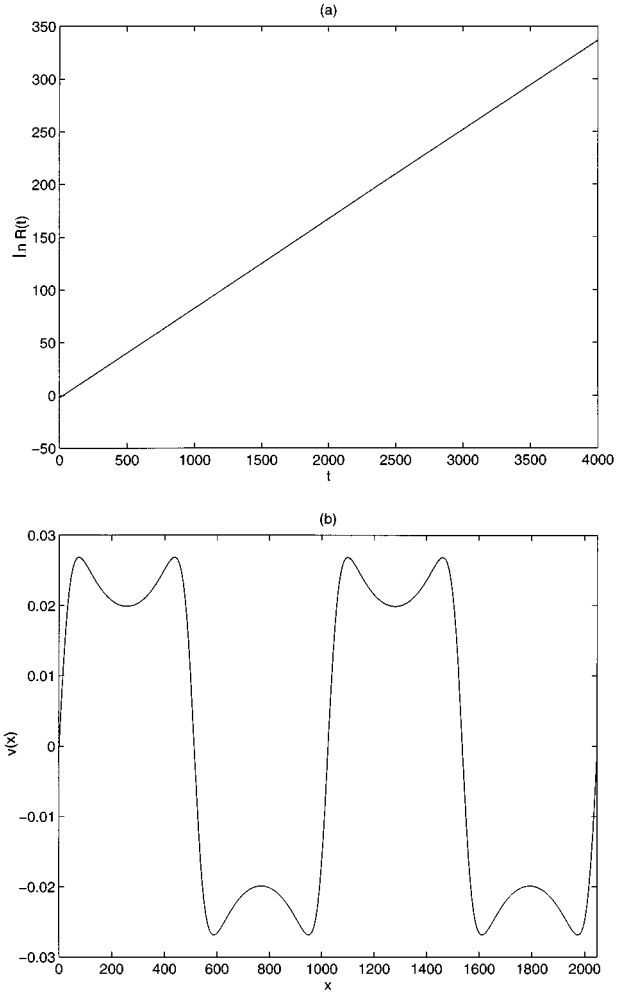

FIG. 5. Linear stability of the steady one-pole solution in a domain of length $L=23\pi$ and wave number $k_0=4$. The initial condition for the perturbation is the function $u_1(x,0)$ (see Sec. V in the text). (a), (b) Simulation with $\mathcal{N}=16\,384$ Fourier modes: (a) the energy of the perturbation versus time, in logarithmic (ln) scale, (b) the corresponding asymptotic mode $v(x)$.

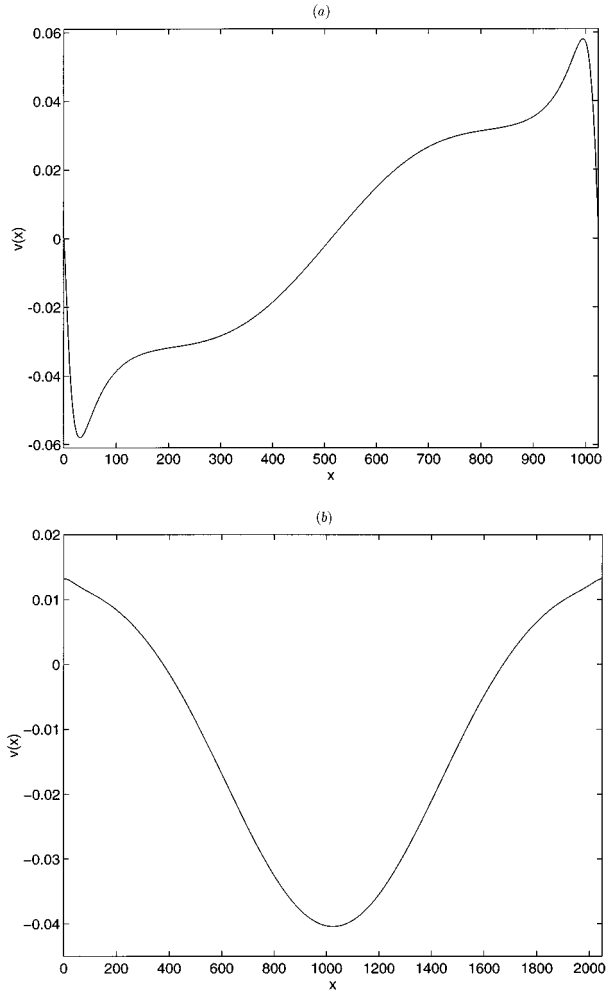

FIG. 6. Linear stability of the steady one-pole solution in a domain of length $L=23\pi$ and wave number $k_0=1$. (a) The initial perturbation is the function $u_2(x,0)$ (see Sec. V in the text); the logarithm of the energy (of the perturbation), $\ln[R(t)]$, is a linear function of time after a short transient; the graph displays the asymptotic mode $v(x)$; (b) the initial condition for the perturbation is the function $u_3(x,0)$ (see Sec. V in the text); again, the logarithm of the energy (of the perturbation), $\ln[R(t)]$, is a linear function of time after a short transient; the graph displays the asymptotic state $v(x)$.

the same. The fact that all initial perturbations lead to the same asymptotic state makes us believe that the unstable eigenspace associated with λ is one-dimensional. (Here, also, we use the terminology of temporal dynamical systems theory.)

Second, we investigate the linear stability of the one-pole solution used as the initial condition in Simulation 4 (see Sec. IV). We recall that this reference state is the one-pole solution ($N=1$, $k_0=1$) in the interval of length $L=23\pi$, stable for the corresponding set of ODE's. Here, we use all three initial conditions $u_1(x)$, $u_2(x,t)$, and $u_3(x)$. Figure 6 summarizes our results for the spatiotemporal behavior of the perturbation $u(x,t)$ when the initial condition is $u_2(x,0)$. Here, as in Fig. 5(a), the energy of the perturbation linearly increases with time, in logarithmic scale. We have considered the two perturbations $u_2(x)$ and $u_3(x)$, finding that the exponents in the two cases are identical up to the seventh digit, i.e., $\beta=2\lambda=0.052\,914$. Figures 6(a) and 6(b) display the two corresponding modes $v_2(x)$ and $v_3(x)$, clearly different in shape. This indicates that the exponent λ is degenerate. In other words, there are (at least) two unstable directions in phase space. Such a two-dimensionality of the unstable eigenspace associated with λ is consistent with the conclusion drawn in Sec. IV from the DNS: two (additional) poles appear simultaneously and the flame front, solution of the PDE (1), jumps from a (coalescent) one-pole steady state to a (noncoalescent) three-pole steady state. In conclusion, the linear stability analysis confirms the results obtained by DNS.

B. Stable steady states

In this paragraph, we present the numerical stability analysis of the two steady states presented in Sec. IV. The first one is the initial condition of Simulation 2, that is, the one-pole ($N=1$, $k_0=1$) steady state in the interval $L=6\pi$. The second one is the asymptotic state reached in Simulations 3 and 4, that is, the coalescent three-pole steady state ($N=3$, $k_0=1$) in the interval $L=23\pi$. In both cases, the exponent tends to $\beta=\lambda=0$, the energy of the perturbation $R(t)$ tending to a constant [see Fig. 7(a) for the three-pole solution; the corresponding graph for the one-pole solution reaches a constant at early times and is, therefore, not shown]. When the initial disturbance is $u_2(x,0)$, the corresponding eigenmodes $v(x)$ are the nonconstant functions shown in Figs. 7(b) and 7(c). For other initial perturbations, we recover the constant mode associated with the invariance of the PDE (1) under shifts of the function F discussed earlier. Finally, the linear stability analysis of the steady two-pole coalescent state ($N=2$, $k_0=1$) for an interval of length $L=14\pi$ is performed; the energy of the perturbation tends to a constant, in a manner similar to the three-pole solution [see Fig. 7(a)]; the asymptotic mode for an initial disturbance $u(x,0)=u_4(x,0)$ is shown in Fig. 7(d). The neutral stability with respect to the ODE's (see Sec. III) persists for the PDE. The shape similarity between the three eigenmodes shown in Figs. 7(b), 7(c), and 7(d) is striking. As the number of poles in the reference state increases, the maximum and minimum of $v(x)$ get closer to the boundaries of the interval.

VI. CONCLUDING REMARKS

In conclusion, most exact steady pole solutions described by a (finite) set of ODE's are unstable for the original PDE. In certain cases, such solutions have been shown to be unstable for the ODE's (such as, e.g., noncoalescent two-pole solutions); in other cases, they are neutrally stable for the ODE's (such as, e.g., two-pole coalescent solutions such that $N\geqslant N_0$). Even when (neutral) stability holds for the ODE's, it usually breaks with respect to the PDE. The only stable steady pole solutions are the coalescent ($N=N_0$)-pole steady state of period L ($k_0=1$). In addition, the stability is neutral. For intervals of small length L such as those reported in this paper [$N_0(L)=1,2,3$], the solution of the PDE is always attracted to a neutrally stable state, that is, the coalescent steady solution containing as many poles as possible, whose period is as large as possible ($k_0=1$) and moving as fast as possible (the front speed is maximal among all possible steady solutions for the interval considered). The migration

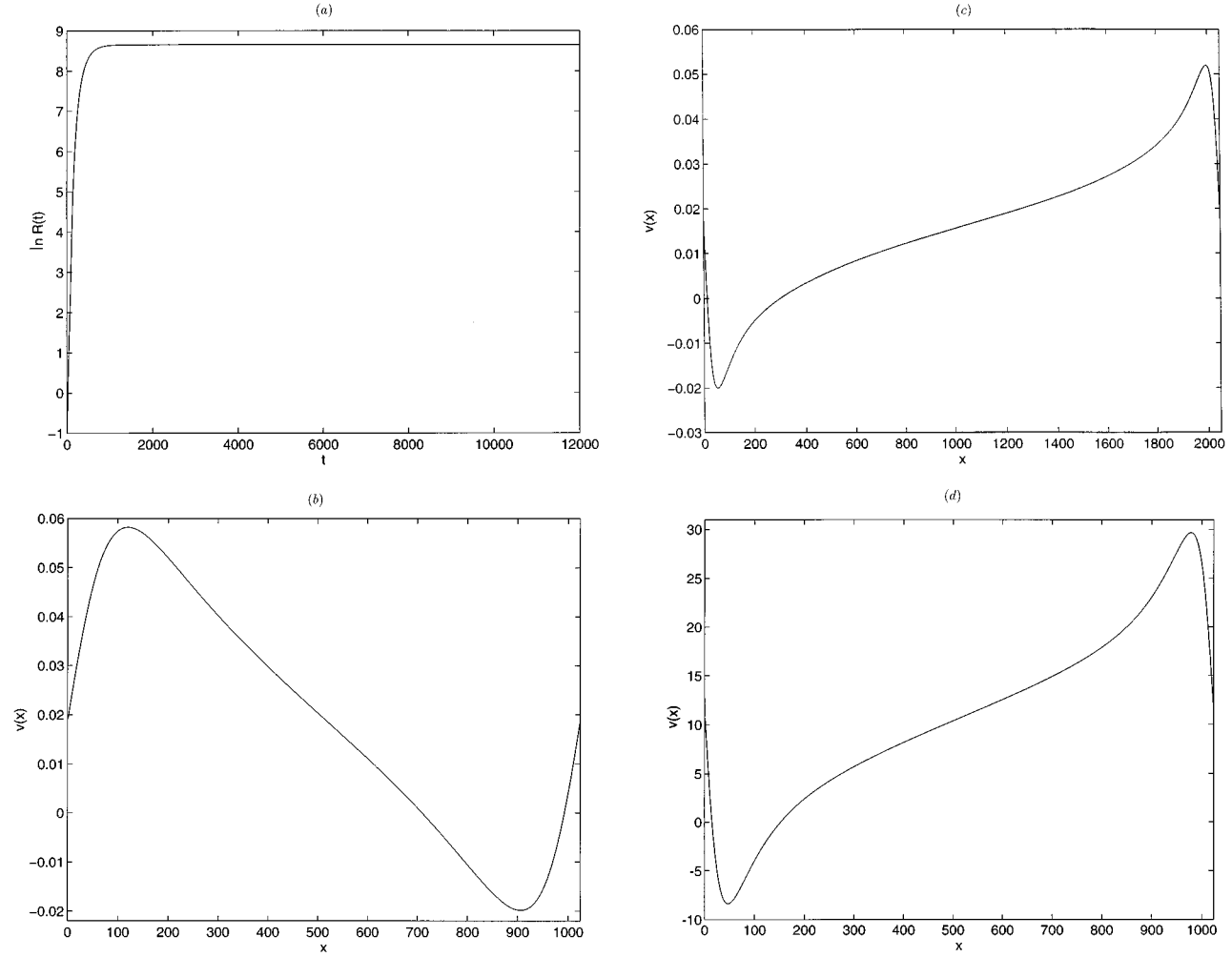

FIG. 7. Linear stability of one-, two-, and three-pole coalescent steady solutions for which the wave number is $k_0=1$. The initial condition for the perturbation is the function $u_2(x,0)$ (see Sec. V in the text). (a)–(c) The initial perturbation is the function $u_2(x,0)$ (see Sec. V in the text). Stability of the one-pole solution for $L=6\pi$ and the three-pole solution for $L=23\pi$: (a) the energy of the perturbation versus time, in logarithmic scale (ln) for the three-pole solution; (b),(c) the asymptotic modes $v(x)$ for (b) the one-pole solution and (c) the three-pole solution. (d) Linear stability of the coalescent two-pole solution for $L=14\pi$. The initial perturbation is the function $u_4(x,0)$ (see Sec. V in the text), the energy of the perturbation is a constant (as a function of time) after some transient, and the graph displays the corresponding asymptotic mode $v(x)$.

to this stable front takes place through various jumps from an exact (steady) pole solution to another one. The stability property of this steady state, however, is lost for intervals of larger size. For instance, we have performed direct numerical simulations over an interval of length $L=82\pi$, starting with the exact coalescent steady ($N=N_0=10$, $k_0=1$)-pole solution. Our results clearly showed that such a state is unstable for the PDE. The instability was also confirmed by carrying out the linear stability study presented in Sec. V. Here, the position of the poles on the imaginary axis, b_j, $j=1,...,10$, was computed by integrating both sets of ODE's (12) and (8) (which gave identical results). This instability (or bifurcation) as the interval length increases, together with the structure of the stable unsteady solutions thus obtained, will be discussed in detail elsewhere. This result is consistent with the numerical simulations reported in [8].

While we were in the final phase of preparing this manuscript, we read the recently published paper [27] in which the stability question of the coalescent steady ($N=N_0$, $k_0=1$)-pole solutions is addressed. (In the numerical study of the previous paper, the authors consider the modified Burger's equation considered in [14], but since the two equations are structurally equivalent, we translate here their finding by using the notation of the present manuscript.) In [27], it is found that the steady states are all neutrally stable, independently of the interval size L considered. There are two major discrepancies between these results and ours. First, at all values of L for which the solution is neutrally stable, we find that the eigenspace associated with the exponent $\lambda=0$ is (at least) two-dimensional. In the notation adopted in [27], this is equivalent to saying $\lambda_0=\lambda_1=0$. Numerical results reported in [27] show that $\lambda_1=0$ only at isolated values of L (where the number of poles N_0 jumps from N to $N+1$). Second, we find that such solutions become unstable as L increases.

Returning to our findings, we would like to emphasize that, although steady pole solutions are exact solutions of the PDE (1), most of these states are unstable for the latter. This, in general, explains why we see them neither in nature, nor in direct numerical simulations. Along these lines, we may recall Landau and Lifschitz's famous words: ''*Yet not every*

solution of the equations of motion, even if it is exact, can actually occur in Nature. The flows that occur in Nature must not only obey the equations of fluid dynamics, but also be stable.''

This, of course, reminds us that any reduction of an infinite-dimensional dynamical system (e.g., a PDE) to a finite-dimensional set of equations (a set of ODE's) should be considered with care. This remark remains valid even if both systems share the same exact solutions and the same invariant subspaces. One has to remember that such solutions and such invariant subspaces may not be stable for the original PDE. This is the case for most exact solutions considered in this paper, as well as the invariant subspace Σ (see Sec. IV), which is also unstable in certain cases.

A similar situation is met in other systems, such as the low-dimensional dynamical systems representing the dynamics of the wall region in turbulent boundary layers [28,29]. First models were restricted to the invariant subspace consisting of flow structures without streamwise variations, i.e., streamwise infinitely elongated streaks. It was shown, however, that such an invariant subspace, together with the solutions lying there, are unstable for most parameter values [29]. The invariant subspace, however, plays a very special role in the more global (stable) intermittent dynamics. The latter, mimicking the bursting events experimentally observed, is due to the presence of homoclinic cycles: the (stable) unsteady solution goes away from the invariant subspace but returns to it in a repetitive fashion.

Likewise, the unstable pole solutions in the flame propagation problem treated in this paper, like those described in [10], play an essential role in the dynamics of the solutions observed by integrating the original PDE: the flame front solution of the full PDE, in general, jumps from one exact pole solution to another one. This study, like that of [10], demonstrates that such jumps are intrinsic phenomena to the PDE. It is thus not necessary to add external noise terms in the PDE to generate them. In the present propagation flame phenomenon, as in many other physical systems [26], the numerical noise, as small as it can be, triggers the inherent instability of most exact solutions.

ACKNOWLEDGMENTS

Two of us (N.A. and M.R.) sincerely thank the Sibley School of Mechanical and Aerospace Engineering at Cornell University for hosting them at the time when this paper was being completed. They also gratefully acknowledge the support of the National Science Foundation (NSF/PYI award MSS89-57462) and the Office of Naval Research, Fluid Dynamics Program (Code 1132F) (Grants N00014-90-J-1554 and N00014-96-0039). G.S. gratefully acknowledges the support of the U.S. Department of Energy (Grant DEFG02-88ER13822), the National Science Foundation (Grant CTS-95-21084), and the U.S.–Israel Binational Science Foundation (Grant 93-00030).

[1] L. D. Landau, Acta Physico Chim. USSR **19**, 77 (1944).
[2] G. Darrieus (unpublished).
[3] G. I. Sivashinsky, Acta Astron. **4**, 1177 (1977).
[4] M. Renardy, Physica D **28**, 155 (1987).
[5] D. M. Michelson and G. I. Sivashinsky, Acta Astron. **4**, 1207 (1977).
[6] D. M. Michelson and G. I. Sivashinsky, Combust. Flame **48**, 211 (1982).
[7] G. Joulin and P. Cambray, Combust. Sci. Tech. **81**, 243 (1992).
[8] S. Gutman and G. I. Sivashinsky, Physica D **43**, 129 (1990).
[9] L. Filyand, G. I. Sivashinsky, and M. L. Frankel, Physica D **72**, 110 (1994).
[10] M. Rahibe, N. Aubry, G. I. Sivashinsky, and R. Lima, Phys. Rev. E **52**, 3675 (1995).
[11] G. Joulin, Phys. Rev. E **50**, 2030 (1994).
[12] G. Joulin, on the mechanisms of wrinkling premixed flames, in *Combustion, Detonation and Shock Waves*, edited by S. M. Frolov (Combustion Institute, Moscow, 1995), Vol. 1.
[13] Y. C. Lee and H. H. Chen, Phys. Scr. **T2**, 41 (1982).
[14] O. Thual, U. Frish, and M. Henon, J. Phys. (France) **46**, 1485 (1985).
[15] S. S. Minaev, Comb. Sci. Technol. **106**, 203 (1995).
[16] U. Frish, Z. S. She, and O. Thual, J. Fluid Mech. **168**, 221 (1986).
[17] G. Hall and J. M. Walt, *Modern Numerical Methods for Ordinary Differential Equations* (Clarendon Press, Oxford, 1976).
[18] C. C. Lin, *The Theory of Hydrodynamic Stability* (Cambridge University Press, New York, 1955).
[19] P. G. Drazin and W. H. Reid, *Hydrodynamic Stability* (Cambridge University Press, Cambridge, 1981).
[20] G. Benettin, Physica D **13**, 211 (1984).
[21] J. P. Eckmann and D. Ruelle, Rev. Mod. Phys. **57**, 617 (1985).
[22] R. Lima and M. Rahibe, J. Phys. A **23**, 781 (1990).
[23] R. Lima and M. Rahibe, J. Phys. A **27**, 3427 (1994).
[24] P. Manneville, in *Macroscopic Modeling of Turbulence Flows*, edited by O. Pironneau, Lecture Notes in Physics Vol. 230 (Springer-Verlag, New York, 1985), p. 319.
[25] L. Keefe, P. Moin, and J. Kim, J. Fluid Mech. **242**, 1 (1992).
[26] L. D. Landau and E. M. Lifshitz, *Fluid Mechanics* (Pergamon, London, 1959).
[27] O. Kupervasser, Z. Olami, and I. Proccacia, Phys. Rev. Lett. **76**, 146 (1996).
[28] N. Aubry, P. Holmes, J. L. Lumley, and E. Stone, J. Fluid Mech. **192**, 115 (1988).
[29] S. Sanghi and N. Aubry, J. Fluid Mech. **247**, 455 (1993).